Vortex pairs formed by tidal currents in the Naruto Strait: Effects of bottom topography, density stratification, and coastline geometry

Tomohiro Nakamura[1], Takuya Yamaguchi[2], Satoshi Nakada[3], Yoshimasa Matsumura[4]

1 Pan-Okhotsk Research Center, Institute of Low Temperature Science, Hokkaido University, Sapporo, 060-0819, Japan
2 Graduate School of Environmental Science, Hokkaido University, Sapporo, 060-0810, Japan. Now at Ehime, Japan
3 National Institute for Environmental Studies, Tsukuba, 305-8506, Japan
4 Atmosphere and Ocean Research Institute, The University of Tokyo, Kashiwa 277-8564, Japan

Corresponding author: Tomohiro Nakamura, nakamura@lowtem.hokudai.ac.jp, Tel:+81-11-706-7494, Fax (office representative): +81-11-706-7142, ORCID: 0000-0001-7632-2733

Keywords: vortex pair or vortex dipole; tidal flow; Naruto Strait; bottom topography and coastline geometry; density stratification; Strouhal number threshold

Abstract

Vortex pairs formed at a strait outlet by tidal flow effectively induce water exchange and material transport in coastal areas. However, the effects of complex bottom topography and density stratification remain unclear. Here, we investigated the development and propagation of vortex pairs in the Naruto Strait, which has complex topography. Satellite observations indicated that the vortex pairs formed on the northern side of the strait continue to move away from the strait after the reversal of tidal flow, shifting their propagation from northward to westward. Numerical experiments revealed that: (1) changes in depth affect the propagation speed and overall size of vortex pairs; (2) density stratification reduces the effects of depth changes; (3) coastline geometry affects the propagation direction of vortex pairs. Furthermore, experiments with idealized topography showed that in a region where depth increases with vortex-pair propagation, the jet decelerates, and the vortex pair shrinks in size. Conversely, in a region where depth decreases, the jet widens, and the vortex pair expands. The changes in jet flow speed can be attributed to flow continuity and depth change, as the latter alters the cross-sectional area. Meanwhile, the changes in vortex pair size and jet width can be explained by vortex propagation on a slope due to potential vorticity conservation. These effects of topography and density stratification may also be significant in other coastal areas and potentially influence the Strouhal number threshold below

which vortex pairs leave an outlet.

Statements and Declarations

There are no conflicts of interest to declare.

1. Introduction

The exchange and transport of water and dissolved and suspended matter through straits and waterways are important for water quality conservation in coastal waters and onshore and offshore nutrient circulation. Tidal currents effectively induce such exchanges through the formation of Eulerian time-averaged flows via tidal rectification (e.g., Robinson 1981; Nakamura et al. 2000) and the generation of net Lagrangian transport even when the Eulerian mean of the flow is zero (Awaji et al. 1980; Awaji 1982). Among them, vortex pairs formed by tidal currents cause particularly effective Lagrangian exchange and transport (Kashiwai 1984; Wells and van Heijst 2003).

A vortex pair (or vortex dipole) is a pair of counter-rotating vortices. As schematically shown in Fig. 1a, a vortex pair translates by self-induced velocity. That is, the vortex on the left side of the schematic (Fig. 1a) induces counterclockwise velocity, forcing the vortex on the right forward. Similarly, the clockwise vortex on the right moves the vortex on the left forward. Combined, the two vortices move each other in the same direction, maintaining the vortex pair. Such a vortex pair can arise from starting vortices generated at a narrow outlet of a strait when tidal flow exits. If the self-induced velocity is sufficiently high compared with the reverse tidal flow, the vortex pair moves away from the strait, transporting water and material in the vortices (Kashiwai 1984; Wells and van Heijst 2003). Such transport by vortex pairs promotes water exchange and material circulation and can affect bottom topography by forming sandbanks due to the transport of suspended particles (Takasugi et al. 1994).

Vortex pair behavior and dynamics have been investigated mainly through laboratory experiments and theoretical analyses and are, thus, limited to quasi-two dimensions (barotropic) and cases with flat bottoms and uniform densities (Kashiwai 1984; Wells & van Heijst 2003; Afanasyev 2006; Nicolau del Roure et al. 2009). However, actual straits can have considerable depth variations and density stratification. For example, the Naruto Strait has a complex bottom topography (Fig. 2), at which vortex pairs are formed by strong tidal flow according to satellite observations (Onishi et al. 1980; Onishi and Nishimura 1980; Nishimura 1986; Nakada et al. 2020). Tidal flow in the Naruto Strait reaches approximately 5 m/s at the maximum (Nanba and Sakaguchi 2005; Takasugi et al. 1990) and forms northward and southward jets in cycles (Nakano 1957; Onishi and Nishimura 1980; Nishimura 1986), causing efficient water exchange (Imasato et al. 1980; Onishi et al. 1980). A vortex pair is positioned ahead of a jet and appears on satellite images as a mushroom-like plume (Fig. 1b). Observation using floats have shown float trajectories consistent with such a structure (Onishi et al. 1980), and consistent flow fields have also been captured using limited current observations (Takasugi et al. 1990).

It remains unclear whether such large depth changes affect the development and propagation of vortex pairs in three-dimensional environments. Furthermore, in an actual strait, not only topography but also density stratification can cause differences from barotropic flow. Therefore, to better understand the behavior of vortex pairs in real seas, this study investigated the formation and development of vortex pairs in the Naruto Strait using satellite observations and numerical experiments, focusing on the effects of bottom topography, density stratification, and coastline geometry on the development and propagation of vortex pairs. The remainder of the paper is organized as follows: Section 2 describes the data used and the setting of the numerical experiments; Sections 3 and 4 present the results of the satellite observation and numerical experiments, respectively; and Section 5 summarizes the results.

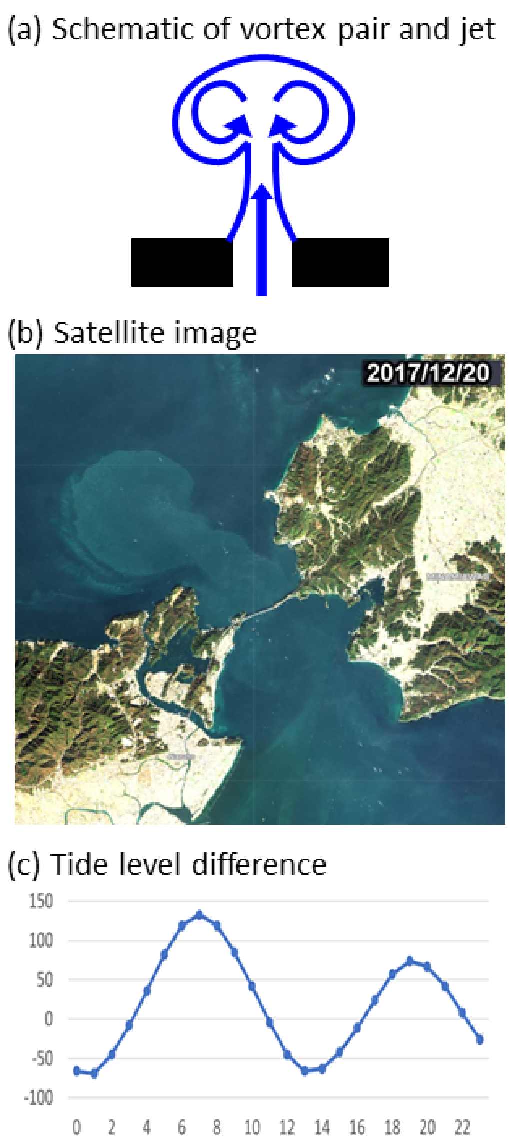

Fig. 1 (a) Schematic diagram of a vortex pair. Arrows denote the currents of the two vortices and a trailing jet, which flows out from a narrow strait between land (black blocks). (b) Satellite image of a vortex pair formed at the Naruto Strait (MSI, Sentinel-2, 20 Dec 2017). A vortex pair appears as a mushroom-like plume. (c) Difference in tidal height (cm) between Fukura and Anaga on the day of the satellite image. The horizontal axis denotes local time (JST).

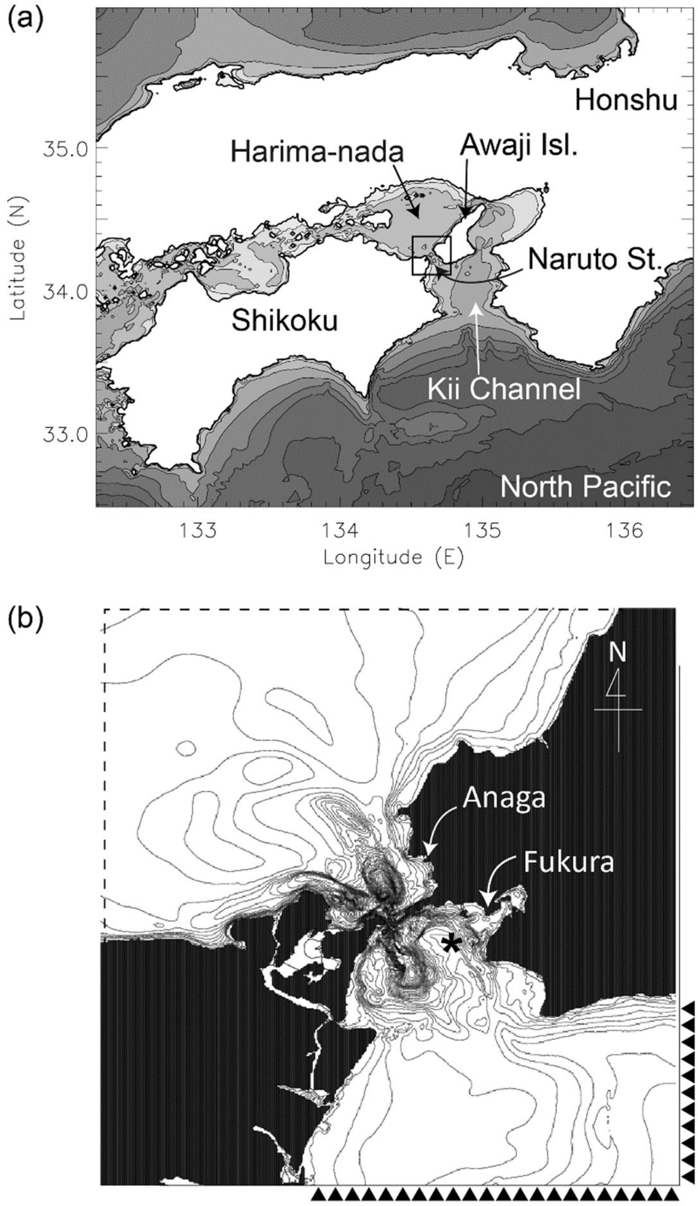

Fig. 2 (a) Map of Naruto Strait. (b) Bottom topography of the Naruto Strait and the model domain. Land is denoted by black areas, and the contour interval is 5 m. The in/outflow and radiation conditions are applied at the boundary with black triangles and dashed lines, respectively. White arrows denote the locations where the tide level was estimated (Fukura in the south, Anaga in the north), and the black asterisk denotes the position of the XBT observation, which was the basis of the model's density stratification.

2. Data and experimental setup

2.1 Satellite and tide level data

To capture vortex pairs using a satellite, we collected color images acquired by the Multispectral Imager (MSI) onboard Sentinel-2. Sentinel-2 provides global coverage satellite images every 5 days with a high spatial resolution of approximately 10 m (Vanhellemont and Ruddick 2016; Nakada et al. 2020). Since Sentinel-2 is in a sun-synchronous orbit, with an equatorial transit local solar time of approximately 10:30 (JST), the satellite images were obtained at approximately 10:40 (JST) in the Naruto Strait. The analysis period was from March 2016 to December 2019.

To estimate the tidal flow when the vortex pairs were captured by the satellite imager, we calculated the difference in tide level between the south and north sides of the Naruto Strait. The tide levels on the north and south sides were estimated at Anaga and Fukura, respectively, located on the Awaji Island side (Fig. 2b). The tidal level difference between these two sites corresponds well with the tidal flow in the Naruto Strait. When the difference (Fukura–Anaga) is positive, the flow is northward, and when negative, it is southward (Nanba and Sakaguchi 2005). The discrepancies between the time of flow reversal estimated from the tide level difference and that observed are mostly within 25 min. The tide level data were obtained from the website of the Hydrographic and Oceanographic Department, 5th Regional Coast Guard Headquarters (https://www1.kaiho.mlit.go.jp/KAN5/tyouryuu/tyouryuu.html).

2.2 Numerical model and experimental setup

The numerical model used was "kinaco" (Matsumura and Hasumi 2008), which is a nonlinear, nonhydrostatic, free surface three-dimensional model with Boussinesq approximation. The model equations include those for potential temperature and salinity to investigate the effects of density stratification. The model domain is shown in Fig. 2b. The Cartesian coordinate system was applied as the domain was small with a width of 27 km in the zonal and meridional directions. The grid size was set to 10 m for all zonal, meridional, and vertical directions but with partial-step cells for the vertical. The model topography was based on M7017 digital bathymetric charts obtained from the Japan Hydrographic Association. The maximum depth was set to 150 m. A horizontal grid size of 10 m is sufficient to resolve topographic features around the Naruto Strait resolved in M7017. A slight change in grid size would yield similar results, considering the length scale of vortex pairs (~5 km) and the width of the deepest sill in the strait (~800 m).

The driving force was in/outflow oscillating sinusoidally with a half-day period (Fig. 3a) because semi-diurnal tides are predominant in the flow of the Naruto Strait. The in/outflow was specified at the eastern and southern boundaries (Fig. 2b), and its amplitude was determined so that the maximum flow speed was approximately 5 m/s in the strait and 4 m/s over the deepest sill. This is between the spring (5 m/s) and neap (2 m/s) tides. Regarding the western and northern boundaries, Orlanski's (1976) radiation condition was applied rather than specifying the in/outflow. This condition is helpful to compute a flow field consistent with the forced in/outflow. The model was initially at rest, and the first tidal period was analyzed. The horizontal viscosity was 1.0×10^{-1} m^2/s, and the vertical viscosity was 1.0×10^{-4} m^2/s. Slip condition was used for the wall and bottom. The results were qualitatively similar to the non-slip condition. Considering the Coriolis parameter f of ~8.3×10^{-5} s^{-1} at 35 °N with a vortex pair length scale of ~5 km and a maximum flow speed of 5 m/s, the Rossby number was approximately twelve. Hence, the effects of the Earth's rotation are small for vortex pairs in the Naruto Strait. We thus set $f = 0$. The results were qualitatively similar when the Coriolis parameter was introduced. It should be noted that the flow field was simplified by omitting spin-up and various forcings, including spring–neap tidal cycles, wind, heat and freshwater fluxes at the sea surface, and the Coriolis term, all of which would affect vortex pairs. Nevertheless, as will be shown in Section 4, the experiments reproduced vortex pairs with similar features to those of satellite images, suggesting that the essential processes for the formation and development of vortex pairs were incorporated.

Table 1 summarizes the experiments conducted to investigate the effects of density stratification and topography. An experiment with a realistic topography and uniform density was conducted as a control. To investigate the effect of density stratification, we conducted an experiment with horizontally uniform stratification and two others with a higher density on the north and south of the sill in the strait (vertically uniform at the initial); to investigate the effect of bottom topography, we conducted an experiment with a flat bottom; and to extract the effect of coastline geometry, we conducted an experiment in which the coastline was deformed with a flat bottom (Fig. 3c). In addition, to extract and investigate the effects of bottom topography, an idealized topography case with a flat bottom was compared with one with an idealized depression (Fig. 3d).

Density stratification was specified based on Japan Oceanographic Data Center (JODC) data. We found only six casts that measured temperature and salinity around the strait archived by JODC: one XBT station in the strait and five CTD stations outside the strait. In the horizontally uniform density-stratification experiment, the vertical profile of temperature was approximated by linear fits for the upper and lower portions to that obtained by XBT (Fig. 3b) on 12 Nov 2008 near the narrowest part in the Naruto Strait at a depth of 90 m (circle in Fig. 2b). Salinity was assumed to be constant at 32.8 psu. In the first experiment with a north–south density difference, density was lower on the south (upstream) and higher on the north (downstream) of the sill in the strait (i.e., the narrowest part). In the second experiment, density was inverted. The temperature and salinity of the lower density water were 17.0 °C and 32.8 psu, while those of the higher density water were 16.0 °C and 33.0 psu, respectively. These salinity values were within the range of the CTD observations near the Naruto Strait. The available CTD data were measured November and December 2007 and 2008—temperature was 16–23 °C, and salinity was ~32.3–33.3 psu. No data on seasonal or interannual variations were found. Thus, seasonal and longer-term variations were not considered here.

Experiment	Bottom topography	Coastline	Density
Control	Realistic	Realistic	Uniform
Density stratification			Horizontally uniform stratification
Density difference 1			Lower on the upstream
Density difference 2			Higher on the upstream
Flat bottom	Flat		Uniform
Deformed coastline		Deformed	
Idealized topography		Rectangular	
Idealized depression	Circular depression		

Table 1 Table of experiments. Blanks denote the same as above.

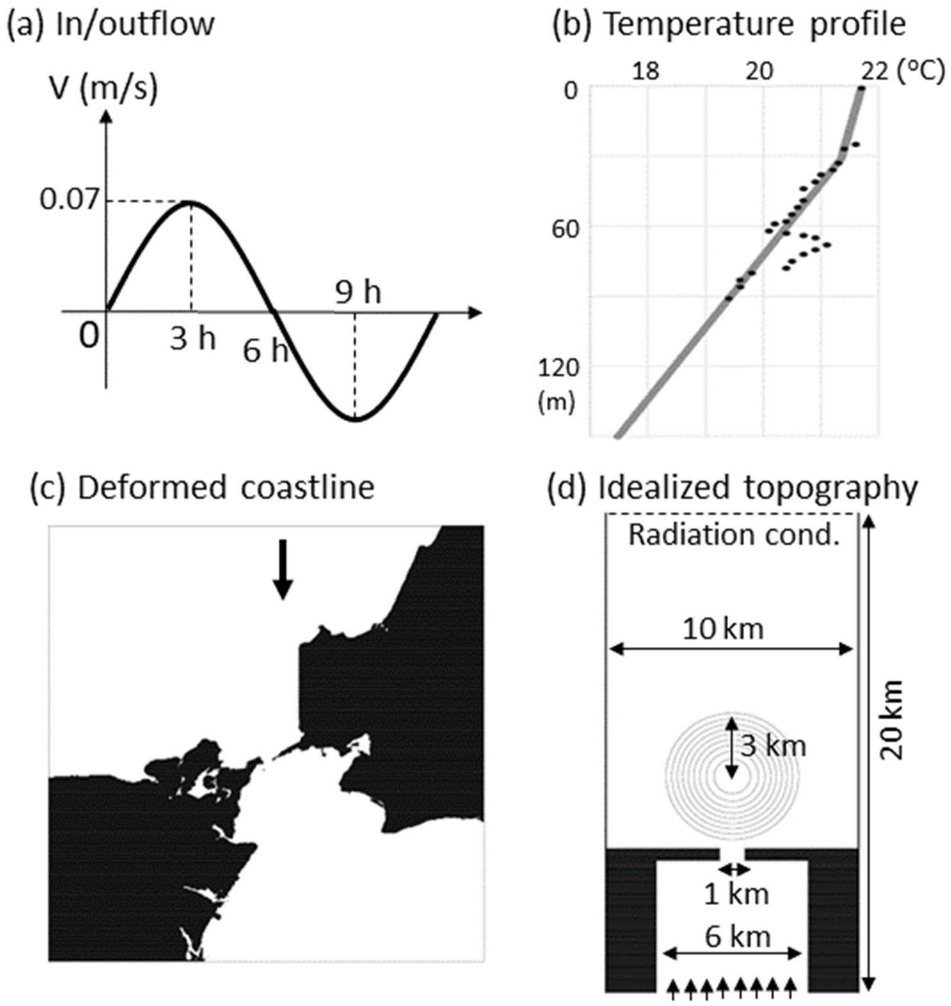

Fig. 3 (a) Schematic diagram of forced in/outflow. (b) Vertical temperature profiles in the model (gray line) and of the XBT observation (black dots; 12 Nov 2008). (c) Deformed coastline geometry, as indicated by the arrow. (d) Idealized topography with a circular depression of 150-m depth.

3. Satellite observation

Vortex pairs were identified through visual inspection of the satellite images. An example is shown in Fig. 1b, in which a mushroom-shaped vortex pair can be recognized based on color difference from the surroundings. Here, the detection of a vortex pair was based on the fact that a vortex pair is formed mainly by the water advected through an outlet, which was, in this case, the narrow outlet (i.e., the narrowest part of the Naruto Strait). As the satellite imager measures ocean color, which is associated with colored substances (suspended and colored dissolved matter, living phytoplankton, bubbles, etc.), the water advected through the narrow outlet can be distinguished when the concentration of colored substances differs on both sides of the outlet (or color changes in the outlet). If such water exhibits a mushroom shape, it is considered a vortex pair. We plotted and overlaid the contours of the detected vortex pairs (Fig. 4a for the north side of the strait and Fig. 4b for the south side). When north- and southward currents occur in the Naruto Strait, vortex pairs are formed on the north (Harima-nada side) and south (Kii Channel side) sides of the strait, respectively. We thus searched for vortex pairs on the north and south sides separately. There were a limited number of clear images due to various issues, including cloud obstruction, and the concentration of river-origin suspended or colored dissolved matter.

The tidal phases were estimated for the vortex pairs in Fig. 4 based on the tide level difference. As exemplified by Fig. 1c, at the time the image in Fig. 1b was captured, the tide level difference between Fukura and Anaga changed from positive (i.e., tide level was higher on the south side and tidal flow was northward) to negative (flow was southward; Fig. 1c). Similarly, the estimated tidal phases ranged from the peak of northward flow to that of southward flow for vortex pairs on the north side. This indicates that after the vortex pairs were formed by the northward tidal flow, they continued to advance during the reverse tide instead of returning to the narrow outlet. On the south side, however, the vortex pairs were found around or before the peak of the southward flow, suggesting they were still in the growing stage. In fact, these were generally smaller than those on the north side (Fig. 4).

The above propagation against the reversed flow is consistent with the Strouhal number for tidal vortex pairs, $S_t = W/(UT)$, where W is the outlet width, U is the tidal flow amplitude, and T is the tidal period. If S_t is less than the threshold value (0.13), vortex pairs escape from an outlet against the reverse tide (Kashiwai 1984; Wells and van Heijst 2003). The S_t for the Naruto Strait is ~0.004–0.009, well below the threshold, where W~800 m, U~2–5 m/s, and T~12.4 h.

Notably, the directions of vortex pair movement and jet differed on the north side; all vortex pairs moved to the west (Fig. 4a), while the jet in the strait was nearly northward (white streaks in Fig. 5). This difference in direction does not fit previous theories or laboratory experiments, which indicated that vortex pairs move in the direction of the jet (e.g., Wells and van

Heijst 2003). The westward movement of the vortex pairs is consistent with past satellite observations (Onishi et al. 1980), and the direction of the jet is consistent with past *in-situ* observations (Nakano 1957; Takasugi et al. 1990), suggesting that the difference in direction occurs always or at least frequently. In contrast, vortex pairs on the south side generally moved straight (Fig. 4b). Considering the notable westward movement on the north side, which differs from what was indicated in past theories and laboratory experiments, and given the limited tidal phases on the south side, we focused on the north side in the following numerical experiments.

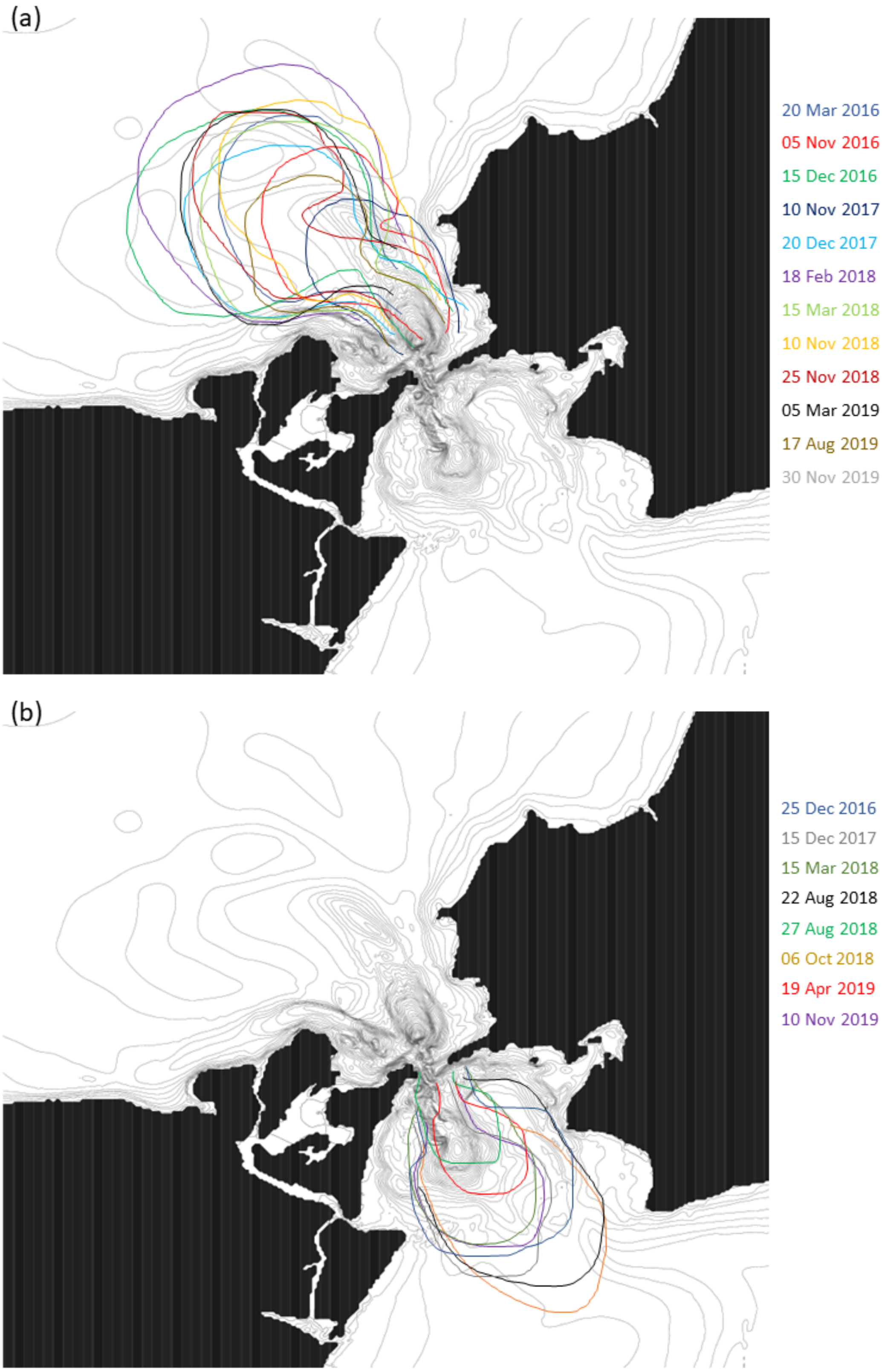

Fig. 4 Contours of observed vortex pairs: (a) north side (Harima-nada) and (b) south side (Kii Channel).

Fig. 5 Satellite image of the northward jet, identified by white streaks (MSI, Sentinel-2, 23 Feb 2018).

4. Numerical experiments

4.1 Uniform density and realistic topography

First, the density was set to uniform (barotropic) as in previous studies, using realistic bottom and coastal topography. Figure 6a shows the distribution of sea surface vorticity 3, 6, and 9 h after the start of the northward flow (after the start of calculation). By definition, a vortex pair can be detected by vorticity. Further, vorticity was a good Lagrangian tracer of the water advected through the strait in our experiments because most vorticity was generated at the narrowest part of the strait, and its damping time scale was sufficiently long. In addition, as we focused on the first tidal cycle, vorticity was not contaminated by that generated in previous cycles.

A vortex pair formed by the northward flow (after 3 h) and developed until the end of the northward flow, moving westward (6 h). Thereafter, the vortex pair did not significantly advance and weakened (9 h), although it did not return to the narrow outlet. Hence, this experiment did not effectively reproduce a major feature of the observed vortex pairs, i.e., the propagation and westward movement after the tide reversed.

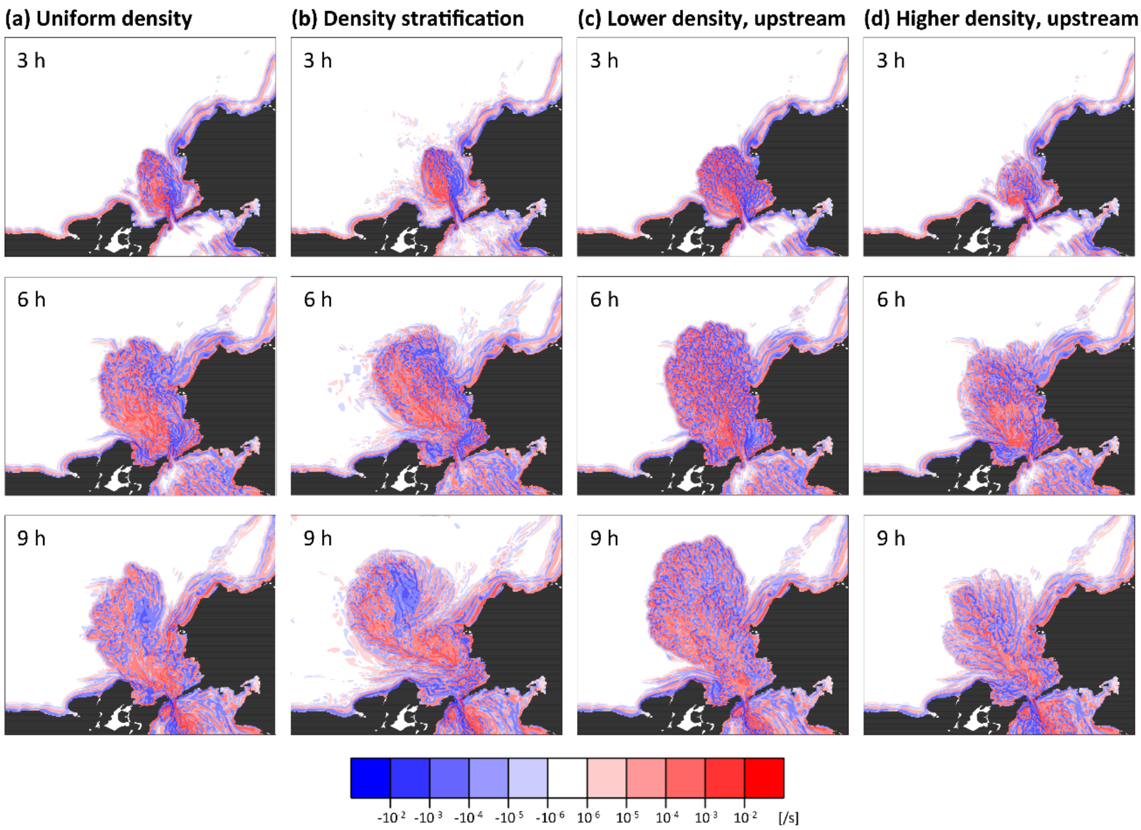

Fig. 6 Horizontal distribution of vorticity (s^{-1}) at the uppermost grid. Experiments on realistic topography with (a) uniform density, (b) horizontally uniform stratification, and north–south

density difference with (c) lower and (d) higher density on the south side. Rows from the top: 3, 6, and 9 h after the start of calculation.

4.2 Effect of density stratification

As the uniform density did not reproduce the characteristics of the observed vortex pairs, we added the effect of density stratification to make the setting more realistic. The experiments were first conducted with horizontally uniform stratification, followed by two cases with horizontal density contrast, where density was lower or higher upstream, respectively.

The experiment with horizontally uniform stratification reproduced the same level of development and movement as observed in the satellite images (Fig. 6b), indicating that density stratification enhanced the development and propagation of the vortex pair. This occurred because density stratification limits or diminishes vertical displacement. In the present case, this effect acted to block currents deeper than the strait sill and confine the currents at shallow depths. In this way, density stratification reduced the effects of bottom topography, enhancing the development and propagation of vortex pairs.

If density stratification works as above, it should have a similar effect if the density upstream of the strait is lower than that downstream (i.e., the water in the vortex pair is lighter than the water below it). In this case, continuous stratification is not necessary, and vertically uniform initial density can exert a similar effect. Thus, we conducted an experiment in which the density was lower on the south side (upstream for north side vortex pairs). The vortex pair indeed became larger and moved farther than the uniform density case (Fig. 6c). It was even larger than the case of horizontally uniform density stratification. The latter difference in development would be due to the difference between approximately two-layer and continuous density stratification because the magnitude of density difference in the two cases was similar. For completeness, the opposite case (a higher density on the upstream) is shown in Fig. 6d. In this case, the development of the vortex pair was at a level similar to the case without stratification (Fig. 6a). The heavier water flowing through the strait tended to sink after passing the sill so that the effect of bottom topography was not mitigated.

The effects of stratification can also be clearly seen in the distributions of sea surface current speed around the narrow outlet (Fig. 7). A jet extended roughly northward from the outlet in all cases, similar to the observations. However, the extension of the jet differed greatly depending on the stratification. The jet extended farther with (Fig. 7b) than without (Fig. 7a) stratification. When the density was lower on the upstream side, the jet extended even farther and spread more (Fig. 7c), whereas when the density was higher upstream, the jet was short on the sea surface (Fig. 7d). These differences in the jet affect the propagation of a vortex pair and suggest that the effects of bottom topography on the jet and vortex pair differ due to stratification.

It should be noted that the maximum current speed was almost the same across all four cases (4.8–5 m/s), and the current speed over the deepest sill (western part of the outlet) was also almost the same (3.7–3.8 m/s at the maximum). Although the simulated current speed was the highest in the eastern part, where there is a shoal, observed current speeds were similar in the western and eastern parts (Nishimura 1986). This is likely due to an overestimation of depth or an underestimation of drag at the shoal. Despite this deficiency, the slight difference in simulated current speed at the outlet confirmed that it is not the cause of the differences in vortex pair development.

These experimental results suggest that bottom topography and density stratification influence the development and propagation speed of vortex pairs. Nevertheless, the westward movement was reproduced in all four experiments, suggesting that another factor is responsible for this movement. A likely candidate is the coastline geometry—a factor common to these cases.

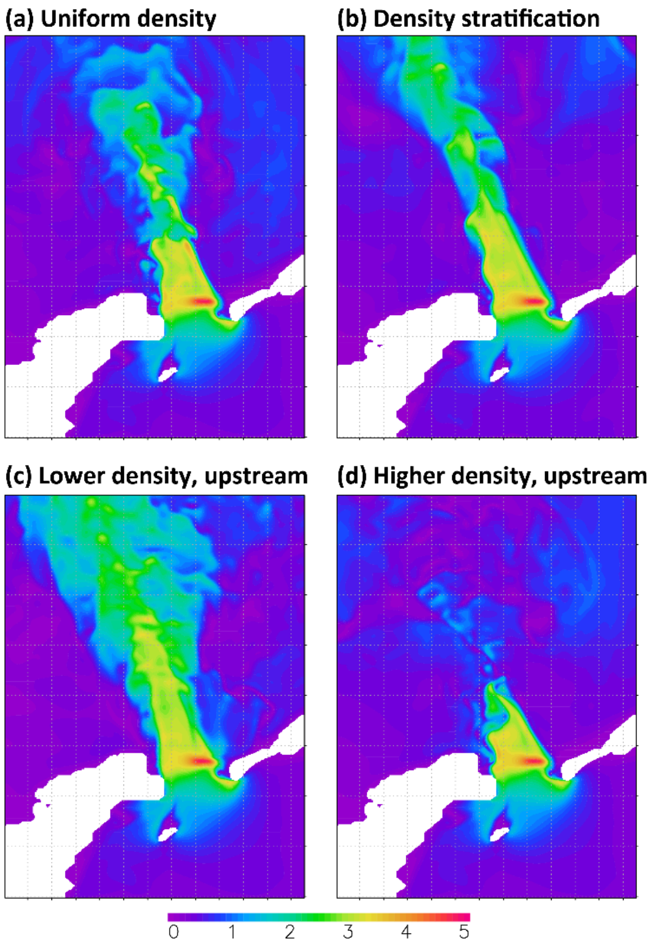

Fig. 7 Current speed (m/s) at the time of maximum northward flow at the uppermost grid around the narrow outlet of the Naruto Strait. Experiments with (a) uniform density, (b) horizontally uniform stratification, and north–south density differences with (c) lower and (d) higher densities

on the south side.

4.3 Effect of topography (uniform density)

To confirm that bottom topography and coastline geometry affect the development, speed, and direction of vortex pairs, we first conducted an experiment with a flat bottom (uniform density). The depth was fixed at 50 m because the deepest point of the sill in the strait is ~50 m.

In the flat bottom experiment, the vortex pair developed more and moved faster than in the realistic topography experiments (Figs. 6 and 8a), although the maximum flow speed was 3.8 m/s in the outlet and almost the same as that over the deepest sill in the realistic topography cases. As expected, the changes in depth weakened the development and movement of the vortex pairs. In the flat bottom experiment, however, the vortex pair developed too much and moved too fast compared to that observed by the satellite, confirming that the observed vortex pairs were weakened by the change in depth, the effect of which was, in turn, reduced by density stratification.

The vortex pair turned westward even in the flat bottom experiment, indicating that the variation in depth was not the main cause of the westward movement. Considering that the vortex pair moved nearly straight in the direction of the jet until it touched the eastern coast, the coastline geometry on the eastern side would be the most likely cause of the westward turn. To determine this effect, we next conducted an experiment in which we cut the protruding part of the eastern coast such that even if the vortex pair moved straight northward, it would not touch the coast (Fig. 3c).

In the deformed coastline experiment, the vortex pair did not move westward (Fig. 8b). Therefore, coastline geometry is the main cause of the westward movement. The associated mechanism is as follows. First, coastal drag weakens the clockwise vortex (negative vorticity) on the shore (eastern) side, so that the offshore counterclockwise vortex (positive vorticity) becomes relatively stronger. Consequently, the self-induced velocity and movement of the vortex pair shift westward.

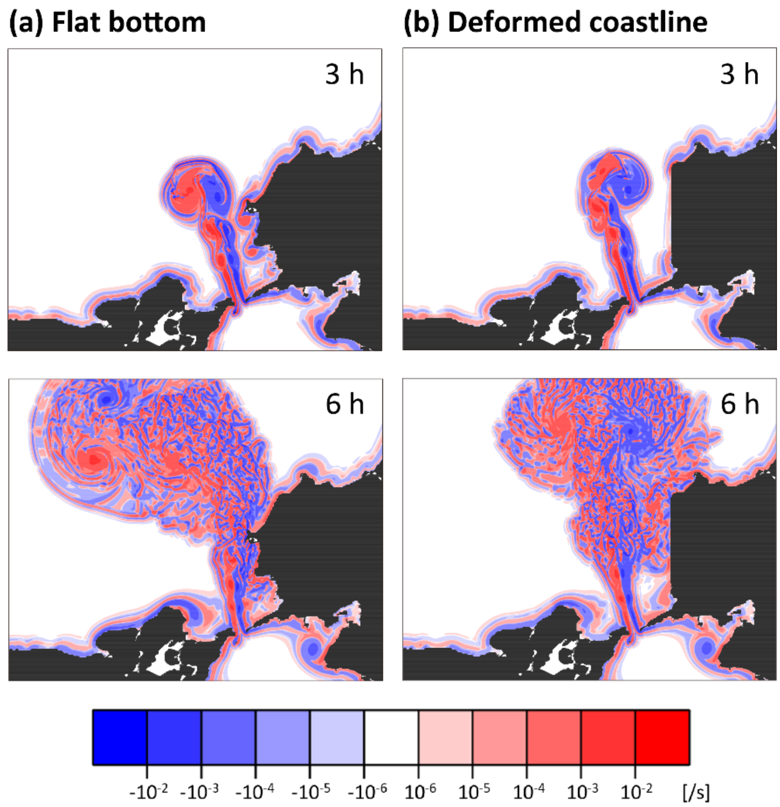

Fig. 8 Distribution of vorticity (s^{-1}) at the uppermost grid. Experiments with a (a) flat bottom and (b) deformed coastline with a flat bottom. Density was uniform in both experiments. From the top: 3 and 6 h after the start of calculation.

4.4 Idealized topography (uniform density)

To investigate how bottom topography influences the development and propagation of vortex pairs, experiments were conducted with idealized topography. Large depth variations in the Naruto Strait occur at three depressions (sea caldrons): two on the north side and one on the south side (Fig. 2b), except for the sill. Among them, we considered the depression through which the northward jet passes. A topography with an idealized strait and a constant depth (50 m) was compared with one with a circular depression of 150-m depth (Fig. 3d). Density was uniform in both experiments.

With the depression, the vortex pair moved slower (Fig. 9), and the jet speed was lower (Fig. 10) than in the case without a depression. This is because as depth increases, the cross-sectional area expands, thereby decreasing the speed of the barotropic jet due to flow continuity. The slowed jet, in turn, weakens the advection of the vortex pair.

Notably, the depression also affected the total size of the vortex pair and the distance between the vortices comprising the pair (Fig. 9). The total size and vortex distance were smaller where the water depth increased as the vortex pair advanced over the depression compared with the case with a flat bottom (Figs. 9 and 10 left). In contrast, the total size and distance were larger, and the jet width was wider in the region of decreasing depth (Figs. 9 and 10 right). This change in distance also reduces the moving speed of the vortex pair because the self-induced velocity of a vortex pair decreases with increasing distance between the centers of the vortices.

We qualitatively considered the change in the distance between the vortices based on the combination of vortex tube advection and potential vorticity conservation (Fig. 11; c.f., Cushman-Roisin 1994). In the present case, the conservation of potential vorticity is:

$$\frac{D}{Dt}\left(\frac{\zeta}{h}\right) \approx 0,$$

where ζ is the (relative) vorticity, h is the depth, and D/Dt is the Lagrangian time derivative. Note that the Earth's rotation is ignored since $|\zeta| \gg f$. This causes the difference in vortex propagation from that which obeys the dynamics of a rotating fluid. By selecting depth as the vertical scale, the following argument focuses on the effects of depth change on barotropic fluids. Viscosity was not important for the length scale of the outlet width as the Reynolds number was ~30,000, and other forcings were not included in these experiments.

First, on the slope where the water deepened as the vortex pair advanced, the vortices moved closer (Fig. 9 left). In a vortex with positive vorticity (counterclockwise) on such a slope (Fig. 11a left), when a vortex tube at an intermediate depth is advected to a shallower depth, it obtains a negative vorticity anomaly ($\Delta\zeta < 0$; clockwise rotation). This is due to the potential vorticity (ζ/h) conservation; ζ decreases (i.e., obtaining a negative anomaly) as h decreases. Conversely, when a vortex tube is advected deeper, it obtains a positive vorticity anomaly ($\Delta\zeta > 0$; counterclockwise rotation). The velocity induced by these vorticity anomalies causes the vortex with positive vorticity to move with the shallow side on its right.

In vortices with negative vorticity (clockwise; Fig. 11a right), a vortex tube that is advected toward shallower waters gains a positive vorticity anomaly (counterclockwise) through the potential vorticity conservation. This is because $|\zeta|$ decreases as h decreases, and hence ζ increases (i.e., obtaining a positive anomaly) as the initial ζ is negative in this case. Conversely, a vortex tube advected toward deeper waters gains a negative vorticity anomaly (clockwise). Accordingly, vortices with negative vorticity are induced to move with the shallow side on their left. In this way, the direction of travel differs depending on the sign of vorticity. This is an interesting feature of the case where the Earth's rotation can be ignored such that the potential vorticity is determined only by the relative vorticity and depth. As a result, the two vortices comprising a vortex pair move closer together, reducing the size of the vortex pair on the slope of this direction (as in Fig. 11a). If this mechanism operates linearly, the vortices may overlap across the jet, partially canceling each other out, and become weaker.

More precisely, as vortex tubes that are advected to intermediate depths should be considered together, vortices with positive and negative vorticity move obliquely to shallower depths rather than following isodepth lines. In both positive and negative vorticity vortices, vortex tubes advected to intermediate depths obtain negative and positive vorticity anomalies on the left and right sides facing the deeper side, respectively. These vorticity anomalies drive the vortices to shallower depths. Taken together, vortices with positive and negative vorticity move diagonally to the direction facing the shallower side to the right and left, respectively, while moving toward the shallower side. The latter slows the advance of the vortex pair.

Contrary to the aforementioned slope, on a slope where the depth became shallower in the direction of vortex pair propagation, the distance between the vortices increased, and the jet width widened (Figs. 9 and 10 right). The mechanism is similar to that described above. Vortices with positive and negative vorticity move with the shallower side to their right and left, respectively (Fig. 11b), through the combined effects of potential vorticity conservation and vortex tube advection. With the direction of the slope reversed, the two vortices that make up the vortex pair move away from each other.

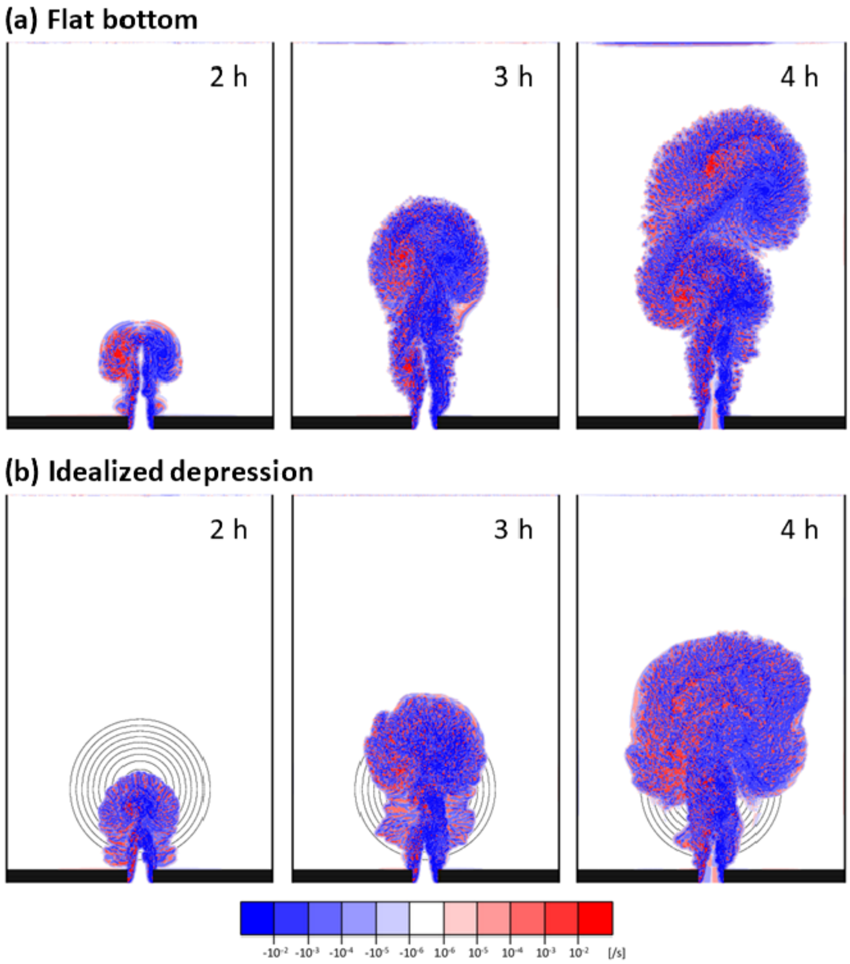

Fig. 9 Horizontal distribution of vorticity (s^{-1}) after 2, 3, and 4 h at the uppermost grid. Experiments with an idealized strait with a flat bottom and uniform density: (a) without and (b) with a circular depression. Contours are isodepths, and black blocks are land.

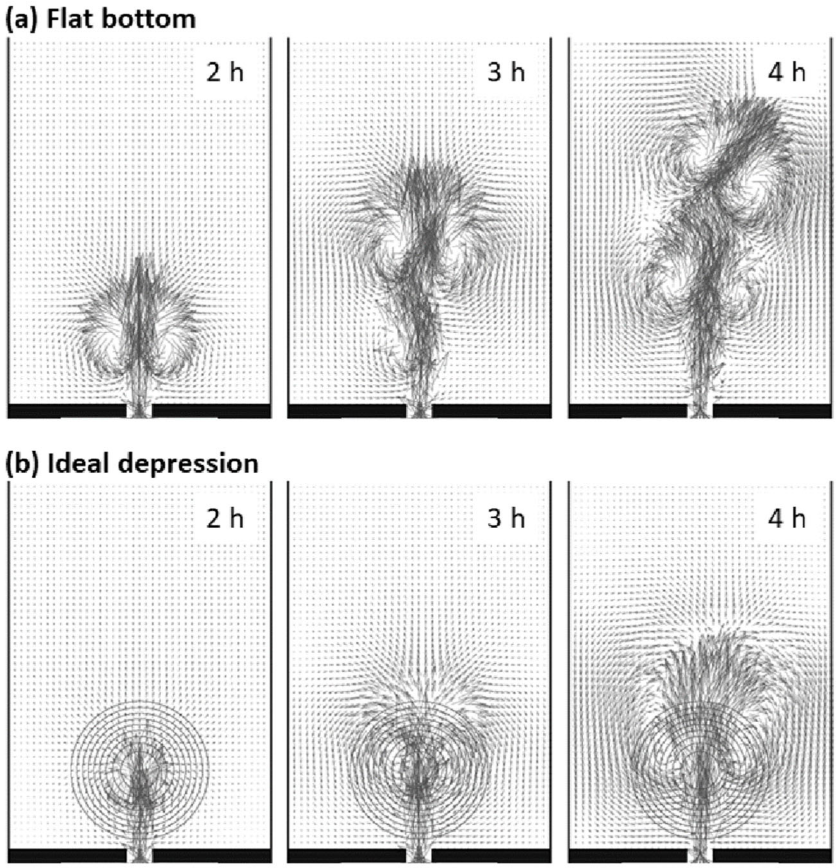

Fig. 10 Same as Fig. 9, but for the velocity vector.

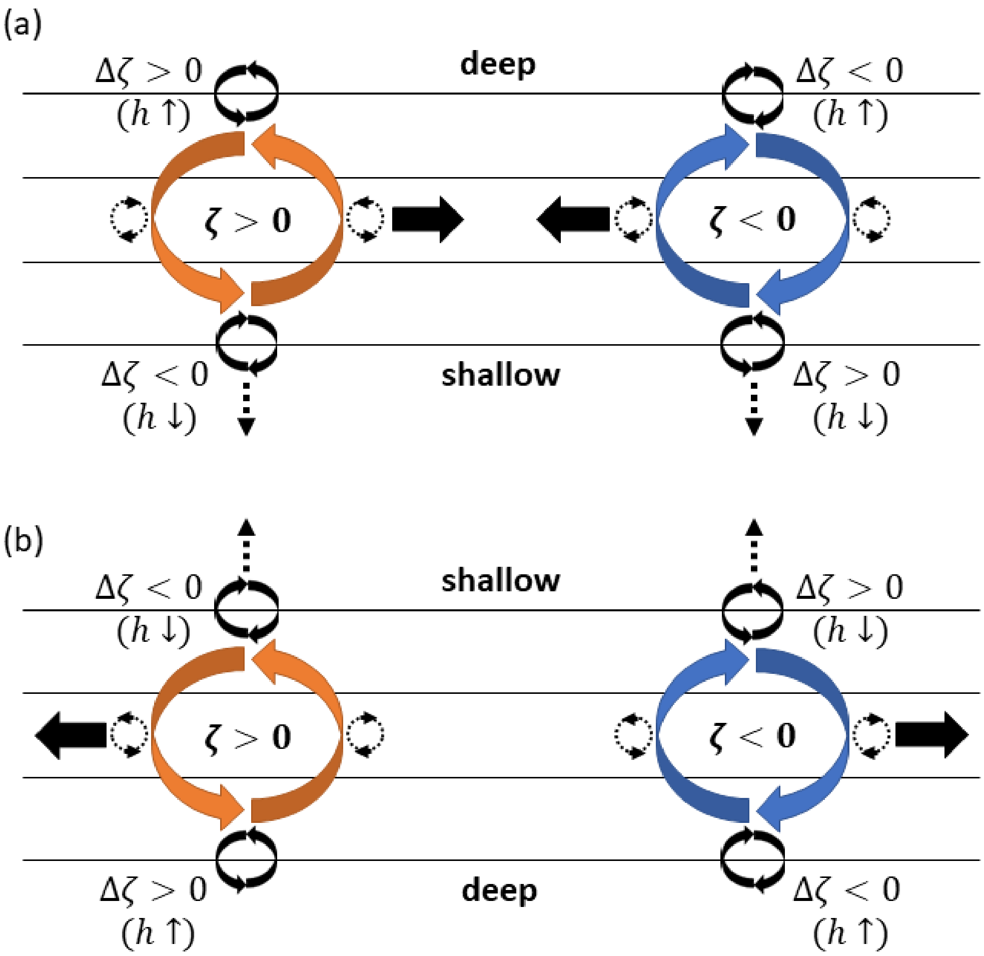

Fig. 11 Schematic diagram of vortex movement due to the effects of potential vorticity (ζ/h) conservation and slope. As the vortex pair moves forward (upward in the figure), the depth becomes (a) deeper and (b) shallower. Solid arrows depict the effect of vortex tubes advected from intermediate depths to shallow and deep depths, while hatched arrows illustrate the effect of vortex tubes advected from deep and shallow depths to intermediate depths.

5. Summary and discussion

We investigated the temporal evolution of vortex pairs in the Naruto Strait using satellite images and numerical experiments. We revealed that the temporal evolution of vortex pairs depends on bottom topography (change in water depth), density stratification (difference in density between vortex pairs and the water beneath them), and coastline geometry. Changes in depth affect the distance between vortices and propagation speed. Density stratification reduces the effects of depth change. Coastline geometry influences the propagation direction of vortex pairs.

With no density stratification, the vortex pairs in the realistic and flat bottom topography experiments were less and more developed and moved slower and faster than observed, respectively. In the experiments with both density stratification and realistic topography, the development of vortex pairs was similar to that observed, i.e., intermediate between the cases of realistic topography and a flat bottom with no stratification. That is, changes in depth in the strait weakened the development and movement of vortex pairs, and density stratification reduced this weakening. In addition, when coastline geometry was deformed so that a vortex pair did not touch the eastern coast, the vortex pair moved straight (almost northward) and did not turn to the west, suggesting that the observed westward movement was caused by coastline geometry.

The idealized topography experiments showed that the depression ahead of the strait outlet (1) slows the flow speed of the jet to delay the propagation of a vortex pair, and (2) the effects of slope on vortex propagation affects the distance between the two vortices comprising a vortex pair and thus the size of the vortex pair and the width of the jet. Specifically, the jet becomes slow, and the distance between the vortices decreases on slopes of increasing depth in the direction of vortex pair propagation, whereas the width of the jet and the distance between the vortices increases on the slope of decreasing depth. The change in jet flow speed can be qualitatively explained by depth change and flow conservation, while the change in the distance between the vortices (or vortex pair size) can be qualitatively explained by the movement of vortices on the slope through potential vorticity conservation.

Although these results suggest the importance of bottom topography and density stratification, previous studies that estimated the Strouhal number threshold did not consider depth change and density stratification (Kashiwai 1984; Wells and van Heijst 2003). In our experiments, the Strouhal number was almost the same (S_t~0.004) for the experiments with realistic bottom topography and those with realistic coastline geometry and a flat bottom (the value was the same within the range of a significant digit regardless of the use of the maximum current speed or the current speed over the main sill). The S_t value is smaller than the threshold value of 0.13; indeed, the vortex pairs did not return to the narrow outlet in all cases. However, although S_t was almost the same, the propagation of vortex pairs differed depending on bottom topography and stratification. This suggests the possibility that the S_t threshold value also depends on bottom topography and stratification.

These effects of topography and stratification would also be important in other areas. Changes in depth are ubiquitous in seas, and density stratification would form if the water is deeper than, e.g., $\sim$10 m for river plumes (and the seawater below) and a few tens of meters for a seasonal thermocline. Since density stratification influences the development and propagation of vortex pairs, it is expected that seasonal and interannual variations in density stratification would cause variations in vortex pairs. Such variation in vortex pairs will lead to variation in water and mass transport. Nevertheless, such seasonal variation was not confirmed in the satellite images analyzed in this study, plausibly due to an insufficient number of images that captured vortex pairs. It should be noted that no detection of vortex pairs in satellite images does not necessarily mean that vortex pairs were not present. As the satellite imager used here measures ocean color, ocean conditions affect the visibility of vortex pairs in addition to atmospheric conditions such as clouds. For example, suspended matter and colored dissolved matter are often supplied from rivers nearby, such as the Yoshino River, and thus vortex pairs would be difficult to be detected when river discharges are low. Repeated *in-situ* observations are needed to clarify the variation of vortex pairs.

In the Naruto Strait, observations showed that vortices with diameters of several meters to tens of meters, called "Uzushio" (whirlpools), are generated and form vortex streets on both sides of the jet, although these were not resolved in the present experiments. In addition, our numerical experiments revealed much smaller-scale perturbations in vorticity than vortex pairs (e.g., Fig. 6). These perturbations are likely produced by instability. These small-scale vortices and perturbations may be important for water mixing. These are left for future research.

Further, the present study considered ideal situations as a first step toward understanding vortex pairs formed in the Naruto Strait. In reality, there is a spring–neap tidal cycle, and vortex pairs would be stronger during spring tides and weaker during neap tides. If the calculated tidal flow reached a quasi-steady oscillation, the flow field would also have vortices and currents generated in previous tidal periods and steady components generated through tidal rectification, in which the Coriolis term could be significant. These would also affect vortex pairs, as well as wind and currents other than tidal currents. In addition, further observations are needed to fully understand vortex pairs in the Naruto Strait. Observations using floats would confirm the presence and reveal the flow field of vortex pairs. Temperature and salinity observations are needed to quantitatively estimate the effects of density stratification, particularly those of seasonal and interannual variations in stratification. Accumulation of satellite images may also be helpful to reveal possible vortex-pair variations associated with a spring–neap cycle, seasonal, and interannual variations. These are also left for future research.

Acknowledgments

This work was supported by JSPS KAKENHI (JP16K05549, JP21K03655, JP22H05204). We also thank anonymous reviewers for their valuable comments.

Data Availability

Satellite images are available from EO Browser, Sentinel Hub, Laboratory for geographical information systems, Ltd., Slovenia (https://apps.sentinelhub.com/eo-browser/). The numerical model (kinaco) is available from Dr. Yoshimasa Matsumura (ymatsu@aori.u-tokyo.ac.jp).

References

Afanasyev, Y. D. (2006) Formation of vortex dipoles. *Phys. Fluids* 18 (3), 9.

Awaji, T. (1982) Water mixing in a tidal current and the effect of turbulence on tidal exchange through a strait. *J. Phys. Oceanogr.* 12, 501–514.

Awaji, T., N. Imasato, and H. Kunishi (1980) Tidal exchange through a strait: A numerical experiment using a simple model basin. *J. Phys. Oceanogr.* 10, 1499–1508.

Cushman-Roisin, B. (1994) Introduction to geophysical fluid dynamics. Prentice Hall, New Jersey.

Imasato, N., T. Awaji, and H. Kunishi (1980) Tidal exchange through Naruto, Akashi and Kitan Straits. *J. Oceanogr. Soc. Jpn.* 36, 151–162.

Kashiwai, M. (1984) Tidal residual circulation produced by a tidal vortex: Part 1. Life-history of a tidal vortex. *J. Oceanogr. Soc. Jpn.* 40 (4), 279–294.

Matsumura, Y. and H. Hasumi (2008) A non-hydrostatic ocean model with a scalable multigrid Poisson solver. *Ocean Modell. (Oxf)* 24 (1), 15–28, doi:10.1016/j.ocemod.2008.05.001.

Nakada, S., I. Morimoto, K. Hasegawa, and S. Tanaka (2020) Visualization of riverine water and vortex dynamics around the Naruto Strait based on high-resolution ocean simulation and satellite images. *J. Adv. Simul. Sci. Eng.* 7 (1), 214–225.

Nakano, M. (1957) On the eddies of Naruto Strait. *Pap. Meteorol. Geophys.* 7 (4), 425–434.

Nakamura, T., T. Awaji, T. Hatayama, K. Akitomo, and T. Takizawa (2000) Tidal exchange through the Kuril Straits. *J. Phys. Oceanogr.* 30, 1622–1644.

Nanba, T. and S. Sakaguchi (2005) Observation report of tidal current in Naruto Strait. *Tech. Bull. Hydrography Oceanogr. Jpn. Coast Guard* 23, 104–111 (in Japanese with English figure captions).

Nicolau del Roure, F., S. A. Socolofsky, and K.-A. Chang (2009) Structure and evolution of tidal starting jet vortices at idealized barotropic inlets. *J. Geophys. Res.* 114, C05024, doi:10.1029/2008JC004997.

Nishimura, T. (1986) Naruto whirlpools. pp.145, K. Sanbunsha Publishers Co., Ltd., Tokyo, Japan (in Japanese).

Onishi, S. and T. Nishimura (1980) Study on vortex current in strait with remote-sensing. 17th International Conference *on* Coastal Engineering 160. 2655–2670.

Onishi, S., S. Tanaka, and T. Nishimura (1980) Study on tidal-exchange phenomena at straits applying remote sensing from Landsat. Proc. Jpn. Soc. Civ. Eng. 298, 63–75 (in Japanese).

Takasugi, Y., T. Fujiwara, T. Higo (1990) Structure of the strong tidal jet in the Naruto Strait. *J. Oceanogr. Soc. Jpn.* 46, 69–83.

Takasugi, Y., T. Fujiwara, and T. Sugimoto (1994) Formation of sand banks due to tidal vortices around straits. *J. Oceanogr.* 50, 81–98.

Robinson, I. S. (1981) Tidal vorticity and residual circulation. *Deep- Sea Res.*, 28A, 195–212.

Vanhellemont, Q. and K. Ruddick (2016) AOLITE for Sentinel-2: Aquatic applications of MSI imagery. ESA Living Planet Symposium. Prague, Czech Republic. 9–13.

Wells, M. G. and G. F. van Heijst (2003) A model of tidal flushing of an estuary by dipole formation. *Dyn. Atmos. Oceans* 37, 223–244.

Figure Captions

Fig. 1 (a) Schematic diagram of a vortex pair. Arrows denote the currents of the two vortices and a trailing jet, which flows out from a narrow strait between land (black blocks). (b) Satellite image of a vortex pair formed at the Naruto Strait (MSI, Sentinel-2, 20 Dec 2017). A vortex pair appears as a mushroom-like plume. (c) Difference in tidal height (cm) between Fukura and Anaga on the day of the satellite image. The horizontal axis denotes local time (JST).

Fig. 2 (a) Map of Naruto Strait. (b) Bottom topography of the Naruto Strait and the model domain. Land is denoted by black areas, and the contour interval is 5 m. The in/outflow and radiation conditions are applied at the boundary with black triangles and dashed lines, respectively. White arrows denote the locations where the tide level was estimated (Fukura in the south, Anaga in the north), and the black asterisk denotes the position of the XBT observation, which was the basis of the model's density stratification.

Fig. 3 (a) Schematic diagram of forced in/outflow. (b) Vertical temperature profiles in the model (gray line) and of the XBT observation (black dots; 12 Nov 2008). (c) Deformed coastline geometry, as indicated by the arrow. (d) Idealized topography with a circular depression of 150-m depth.

Fig. 4 Contours of observed vortex pairs: (a) north side (Harima-nada) and (b) south side (Kii Channel).

Fig. 5 Satellite image of the northward jet, identified by white streaks (MSI, Sentinel-2, 23 Feb 2018).

Fig. 6 Horizontal distribution of vorticity (s^{-1}) at the uppermost grid. Experiments on realistic topography with (a) uniform density, (b) horizontally uniform stratification, and north–south density difference with (c) lower and (d) higher density on the south side. Rows from the top: 3, 6, and 9 h after the start of calculation.

Fig. 7 Current speed (m/s) at the time of maximum northward flow at the uppermost grid around the narrow outlet of the Naruto Strait. Experiments with (a) uniform density, (b) horizontally uniform stratification, and north–south density differences with (c) lower and (d) higher densities on the south side.

Fig. 8 Distribution of vorticity (s^{-1}) at the uppermost grid. Experiments with a (a) flat bottom and (b) deformed coastline with a flat bottom. Density was uniform in both experiments. From the top: 3 and 6 h after the start of calculation.

Fig. 9 Horizontal distribution of vorticity (s^{-1}) after 2, 3, and 4 h at the uppermost grid. Experiments with an idealized strait with a flat bottom and uniform density: (a) without and (b) with a circular depression. Contours are isodepths, and black blocks are land.

Fig. 10 Same as Fig. 9, but for the velocity vector.

Fig. 11 Schematic diagram of vortex movement due to the effects of potential vorticity (ζ/h) conservation and slope. As the vortex pair moves forward (upward in the figure), the depth becomes (a) deeper and (b) shallower. Solid arrows depict the effect of vortex tubes advected from intermediate depths to shallow and deep depths, while hatched arrows illustrate the effect of vortex tubes advected from deep and shallow depths to intermediate depths.

List of Tables

Table 1 Table of experiments. Blanks denote the same as above.